Nature of a Long Carbon–Carbon Bond Beyond 2.0 Å

Takashi Kubo (kubo@chem.sci.osaka-u.ac.jp)
Osaka University https://orcid.org/0000-0001-6809-7396
Yuki Suga
Osaka University
Daisuke Hashizume
RIKEN https://orcid.org/0000-0001-7152-4408
Hiroki Suzuki
University of Tokyo
Tatsuya Miyamoto
University of Tokyo
Hiroshi Okamoto
University of Tokyo
Ryohei Kishi
Osaka University https://orcid.org/0000-0002-6005-7629
Masayoshi Nakano
Osaka University https://orcid.org/0000-0002-3544-1290

Article

Keywords: carbon–carbon single bonds, fluorenyl rings, molecular orbital

Posted Date: March 23rd, 2021

DOI: https://doi.org/10.21203/rs.3.rs-320873/v1

Nature of a Long Carbon–Carbon Bond Beyond 2.0 Å

Takashi Kubo[1]*, Yuki Suga[1], Daisuke Hashizume[2]*, Hiroki Suzuki[3], Tatsuya Miyamoto[3,4], Hiroshi Okamoto[3,4], Ryohei Kishi[5], and Masayoshi Nakano[5]

[1]Graduate School of Science, Osaka University, Toyonaka, Osaka 560-0043, Japan

[2] RIKEN Center for Emergent Matter Science (CEMS), Wako, Saitama 351-0198, Japan

[3] Department of Advanced Materials Science, University of Tokyo, Kashiwa, Chiba 277-8561, Japan

[4] National Institute of Advanced Industrial Science and Technology (AIST)-University of Tokyo Advanced Operando-Measurement Technology Open Innovation Laboratory (OPERANDO-OIL), AIST, 5-1-5 Kashiwanoha, Kashiwa, Chiba 277-8561, Japan

[5]Graduate School of Engineering Science, Osaka University, Toyonaka, Osaka 560-8531, Japan

*Corresponding author. Email: kubo@chem.sci.osaka-u.ac.jp (T.K.); hashi@riken.jp (D.H.)

Abstract

Elongating carbon–carbon (C–C) single bonds is challenging in terms of molecular design and synthesis, and in understanding the nature of the long bonds. Herein, we demonstrate that a C–C bond longer than 2.0 Å can be realised by face-to-face interactions between fluorenyl rings. A small orbital overlap between the distantly positioned carbon atoms is observed as a small concentration of electrons on the X-ray electron density maps. The highest occupied molecular orbital (HOMO) and the lowest unoccupied molecular orbital (LUMO) of the compound originate from the in-phase and out-of-phase interactions of the overlapping orbitals, respectively, with a gap of 2.39 eV. Solid-state ^{13}C NMR spectroscopy shows a sharp peak at 82.9 ppm for the long-bonded carbons, while a CASSCF(6,6) calculation indicates a small diradical character. The experimental and theoretical analyses reveal a sufficient covalent bonding character in the long C–C bond.

Introduction

The covalent bond is one of the most fundamental concepts in organic chemistry, wherein the strength of a covalent bond depends on the extent of the overlap integral between the orbitals of the atoms sharing the pair of electrons. The deviation from standard structures caused by the stretching, twisting, or bending of bonds leads to a reduction in the overlap of orbitals between atoms, and so the question of whether atoms in a special state are bonded or not is an important issue when defining covalent bonds. More specifically, bond elongation has played an important role in learning the limits of covalent bonds[1–7], and recent studies on compounds possessing long C–C single bonds[8–15] have provided more a detailed understanding of covalent bonds. In particular, electron density analysis suggests that a C–C bond with a distance of ~1.9 Å is in the boundary region of covalent bonding[14]. Herein we report the synthesis and characterisation of a fluorenyl-based hydrocarbon compound **1**, in which a sufficiently large covalent bonding interaction is present between carbon atoms, even with an interatomic distance of 2.04 Å.

Results and discussion

Compound **1** (**Fig. 1**), which contains a long C–C bond, was prepared over four steps from commercially available 9-fluorenone, as outlined in **Scheme S1**. More specifically, deprotonation of the dihydro-precursor (**2**) led to a dianionic species (**3**), which adopted a C_3-symmetric propeller-like structure, as confirmed by ^{1}H NMR spectroscopy and X-ray crystal structural analysis (**Figs. S1** and **S2**, respectively). The two-electron oxidation of **3** with *p*-chloranil afforded neutral compound **1** as dark purple crystals, which were sparingly soluble in common organic solvents. Crystals stored under air at room temperature for two years showed no appreciable decomposition. X-ray crystal structure analysis revealed that the two fluorenyl rings in **1** adopt a face-to-face alignment, instead of a propeller-like structure (**Fig.**

1b), and a distant C–C interatomic contact was found between the carbon atoms (C2 and C3 in **Fig. 1b**) at the 9-positions of the face-to-face fluorenyl rings. Based on single crystal X-ray analysis, the C–C distance was determined to be 2.0415(5) Å at 90 K, and this distance was well reproduced (2.0478 Å) by density functional theory (DFT) calculations at the B3LYP-D3/6-311+G** level of theory (see Table S1 for a DFT benchmark study). This level of calculation using the optimised geometry also successfully reproduced the Raman spectrum measured at 100 K (**Fig. S3**). Furthermore, the Hirshfeld's rigid bond test[16] and difference Fourier analysis on the structure of **1** (90 K) derived from refinement of the high-order diffraction data indicated that the observed C–C distance of >2.0 Å is an intrinsic feature, and is not a result of structural disorder (see the SI for the high-order refinements and analyses). The geometries around C2 and C3 are planar and the sum of the bond angles surrounding C2 and C3 are 359.92 and 359.87°, respectively, thereby suggesting their sp^2 hybridisation. Considering that the parent fluorenyl radical possesses a large spin density of >0.5 at the 9-position[17], an appreciable electron–electron interaction appears to be present between C2 and C3.

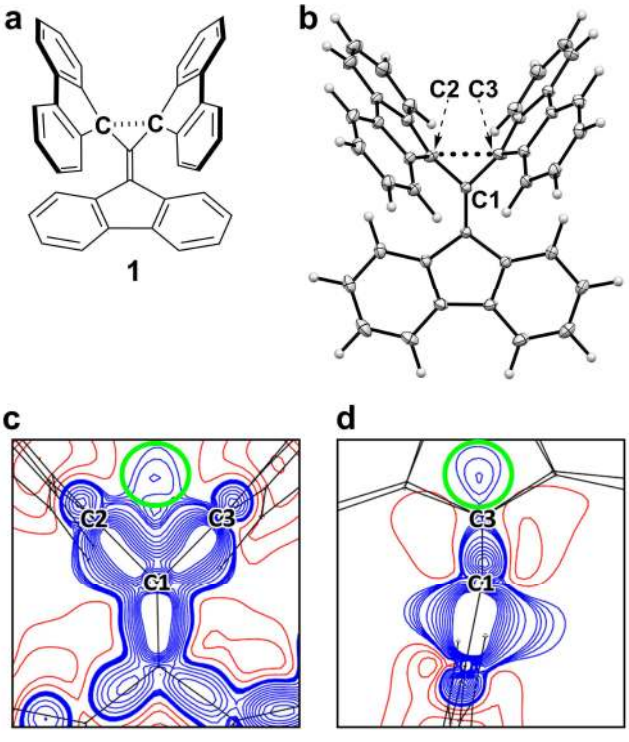

Fig. 1. Structure of 1. **a**, Chemical structure of **1**. **b**, An ORTEP drawing of **1** at 90 K. Thermal ellipsoids are drawn at the 50% probability level. **c**, Static model deformation density maps on the C1-C2-C3 plane, and **d**, cross-sectional view of the C1-C2-C3 plane along the line connecting C1 and the midpoint between the C2 and C3 atoms. The concentration of electron density between C2 and C3 is marked by a green circle. The blue lines represent positive contours from 0.01 to 0.05 e $Å^{-3}$ in steps of 0.01 e $Å^{-3}$ and from 0.10 to 0.50 e $Å^{-3}$ in steps of 0.05 e $Å^{-3}$. The red lines represent negative contours from −0.05 to −0.50 in steps of −0.05 e $Å^{-3}$.

To gain deeper insight into the electronic interaction between C2 and C3, we performed electron density distribution (EDD) analysis to visualise the distribution of valence electrons in the crystalline state[18]. The single-crystal X-ray diffraction data of **1** were obtained up to $[\sin\theta / \lambda]_{max}$ = 1.11 $Å^{-1}$ using Mo Kα radiation at 90 K. **Figures 1c** and **1d** show the static model deformation density maps[19,20] of **1** (90 K) on the C1-C2-C3 plane and the cross section of the C1-C2-C3 plane through the skeletal carbons. A concentration of electron density (peak height ≈ +0.03 e $Å^{-3}$, green circle in **Figs. 1c** and **1d**) is apparently recognised between C2 and C3, indicating orbital overlap that allows the sharing of electrons in the C2–C3 region. The deformation electron density lies outside the line connecting C2 and C3, like the bent bond of cyclopropane. This observation strongly supports the existence of a sufficient covalent bonding interaction between C2 and C3. Indeed, the height of the electron density corresponds to the Bader's bond order[21] of 0.26. The Wiberg bond index (WBI) of 0.485, as derived from natural bond orbital (NBO) analysis based on the DFT calculations of **1** (90 K) at the B3LYP-D3/6-311+G** level of theory, also supports the presence of a large bonding interaction. The strength of the covalent bonding interaction, which was estimated from the singlet–triplet vertical excitation energy (ΔE_{S-T}) by a B3LYP-

D3/6-311+G** calculation of **1** (90 K), reached up to 138 kJ mol^{-1}. Within the Heitler–London approximation, the covalent term K can be described as half the ΔE_{S-T}. Therefore, the covalent bonding interaction of **1** (90 K) remains sufficiently large in comparison to that of multicentre long bonds (pancake bonds) in π-dimers of radical species[22,23]. On the other hand, the atoms-in-molecules (AIM) analysis[24] based on the experimental EDD indicated the lack of a bond critical point (BCP) between C2 and C3 despite the presence of a positive deformation electron density. AIM analysis based on the theoretical electron density, which was determined by a B3LYP-D3/6-311+G** calculation[25] based on the X-ray structure at 90 K, also showed no BCP between C2 and C3. In a three-membered ring with one elongated C–C bond, the BCP and ring critical point (RCP) of the elongated bond approached one another in position and in value, resulting in the disappearance of the critical points due to the coalescence of the negative (of BCP) and positive (of RCP) curvatures of the charge density[21].

To further understand the bonding nature between C2 and C3, the optical conductivity (σ) was determined by the Kramers-Kronig transformation of the polarised reflectivity spectra obtained at 100 K. The value of σ is related to the absorption coefficient (α) of a material according to the equation $\sigma = \alpha nc$, where n is the refractive index and c represents the speed of light. The polarisation of light along the line connecting C2 and C3 (i.e., the a-axis direction, see **Fig. S4** for the unit cell) on the (001) face of a single crystal resulted in an intense peak at 518 nm (**Fig. 2a**). DFT calculations for **1** (90 K) at the B3LYP-D3/6-311+G** level of theory indicated that the HOMO and LUMO of **1** (90 K) originate from in-phase and out-of-phase interactions of the singly occupied molecular orbitals (SOMOs) of the parent fluorenyl radical, respectively, and are mainly distributed on C2 and C3 (**Fig. 2b**). Time-dependent (TD) B3LYP-D3/6-311+G** calculations for **1** (optimized at the B3LYP-D3/6-311+G** level) revealed that the intense peak at 518 nm is assignable to the optically

allowed HOMO→LUMO transition (**Fig. S5**). Thus, the electronic interaction between C2 and C3 causes a large orbital splitting of 2.39 eV (= 518 nm).

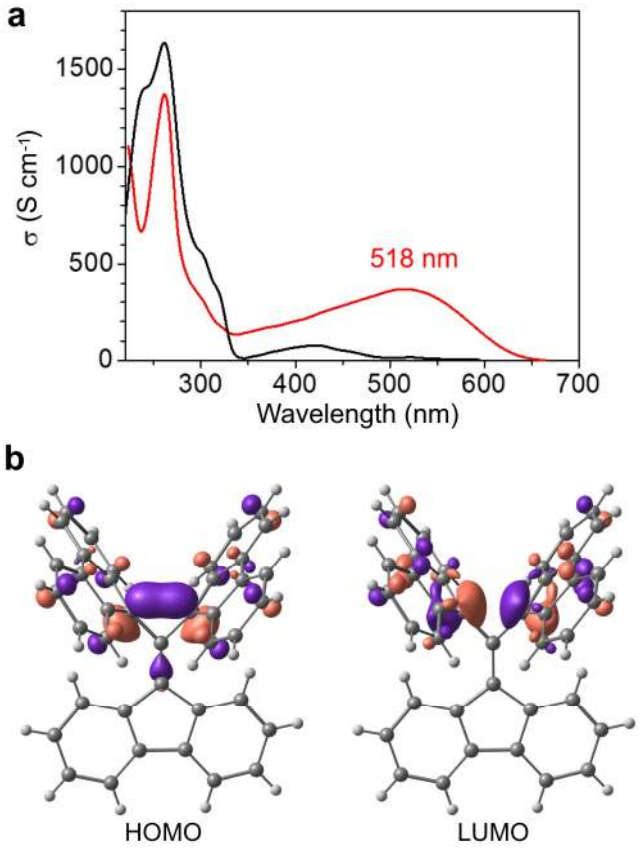

Fig. 2. Evaluation of the electron–electron interaction between C2 and C3. a, Optical conductivity (σ) spectra of **1** at 100 K obtained with light polarised along (red solid line) and perpendicular to (black solid line) the *a*-axis on the single crystal (001) face. **b**, HOMO and LUMO of **1** (90 K) calculated using the B3LYP-D3/6-311+G** method. Purple and light red surfaces represent the relative signs of the orbital coefficients drawn at the 0.4 e $Å^{-3}$ (= 0.06 e au^{-3}) level.

The π-orbital axis vector (POAV1) analysis method, which involves a structural deformation analysis of a sp^2 carbon atom from planarity[26], was employed for the examination of **1** (90 K), and yielded pure sp^2 hybridisation for both C2 ($sp^{2.003}$) and C3 ($sp^{2.002}$). This hybridisation state is fully consistent with the NBO analysis, thereby indicating

that the orbitals involved in the bonding interaction between C2 and C3 possess almost pure 2*p* character (*p*% = 98% for C2 and C3). However, the hybridisation state estimated from these analyses was not in line with the ^{13}C NMR chemical shifts of C2 and C3. More specifically, the cross polarisation/magic angle spinning (CP/MAS) ^{13}C NMR spectrum of powdered **1** at 100 K gave a peak at 82.9 ppm (**Fig. 3a**). This peak was assigned to C2 and C3 based on the fact that the empirically scaled[27] gauge-independent atomic orbital (GIAO)[28,29] B3LYP-D3/6-311+G** calculation for **1** (optimized at the B3LYP-D3/-311+G** level) gave a value of 88.2 ppm for C2 and C3 (**Fig. S6**). The upfield position of the signals of C2 and C3, relative to those of other sp^2 carbon atoms, implies that these carbon atoms are not purely sp^2-hybridised, but bear more *p* character, as determined by the fact that the ^{13}C chemical shifts of C2 and C3 are comparable to those of sp^3 carbon atoms in other long C–C σ-bonds[5,7,13,30,31] (**Fig. 3b**). It is notable that no signal broadening of the peak at 82.9 ppm was observed, thereby suggesting the small diradical character of **1**. Indeed, the CASSCF(6,6)/6-311G* calculation of **1** (90 K) gave a natural orbital occupancy number (NOON)[32] of 0.128 (i.e., a diradical index, y_0, of 12.8%) for the lowest-unoccupied natural orbital (LUNO).

A through-bond interaction may be involved in the electronic interaction between C2 and C3, as indicated by the distribution pattern of the HONO and LUNO for **1** (90K, **Fig. S7**). This is similar to the distribution pattern of the two-configuration (TC) SCF orbitals for *m*-benzyne[33,34], in which a through-bond interaction stabilises the symmetric bonding molecular orbital. In the case of **1**, the 2*p* orbitals on C2 and C3 have a dominant through-space interaction, with a small contribution from the through-bond interaction between the 2*p* orbitals and the σ-orbitals of the C1–C2/C1–C3 bonds.

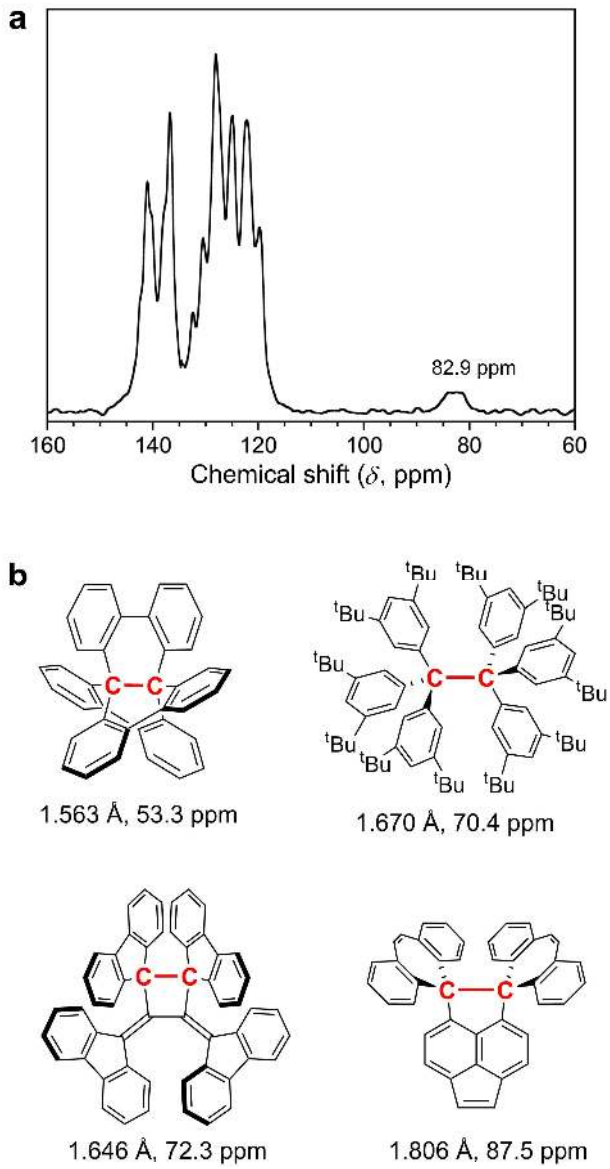

Fig. 3. ^{13}C NMR chemical shifts. a, Solid-state CP/MAS ^{13}C NMR spectrum of powdered **1** measured at 100 K. **b**, Bond distances and ^{13}C chemical shifts at the sp^3 benzylic carbons (shown in red) of selected aromatic hydrocarbon compounds.

We then investigated the temperature dependence of the C2–C3 interatomic distance ($d_{C2\text{-}C3}$) by variable-temperature X-ray diffraction measurements. As shown in **Fig. 4a**, $d_{C2\text{-}C3}$ decreased with increasing temperature, and levelled off at temperatures >300 K. Generally, upon heating, the majority of molecular crystals exhibit positive thermal expansion along with molecular bond elongation. Indeed, the unit cell volume of **1** gradually increased upon

heating between 90 and 400 K, and a significant change in the *c*-axis direction was observed (**Fig. S8**). However, as indicated above, $d_{C2\text{-}C3}$ was found to decrease upon heating. The unusual thermal change in $d_{C2\text{-}C3}$ likely arose from the interlocked dimeric structure shown in **Figs. 4c** and **S4**. At lower temperatures, the crystal of **1** shrinks like a normal material, bringing the two molecules in the dimeric pair closer together. As a result, the two fluorenyl rings of a single molecule are spread out upon the approach of a fluorenyl ring from the other molecule (see **Fig. S9** for a schematic representation), resulting in negative thermal effect on $d_{C2\text{-}C3}$. It is notable that the temperature dependence of $d_{C2\text{-}C3}$ is small at temperatures >300 K, whereas the interatomic distance ($d_{C1\text{-}C1}$) between the C1 atoms in the dimeric pair steadily increases upon heating, even beyond 300 K (**Figs. 4b** and **4c**). This result suggests that the intrinsic distance between C2 and C3 is ~1.98 Å and that the elongation of $d_{C2\text{-}C3}$ at low temperatures originates from the crystal packing effect.

Due to the long interatomic distance between C2 and C3, progressive changes were observed in the HOMO→LUMO transition (**Figs. 4d** and **S10**), ^{13}C NMR chemical shift (**Figs. 4e** and **S11**), Wiberg bond index (**Fig. 4f**), singlet–triplet energy gap (**Fig. 4g**), and diradical character (**Fig. 4h**). These results indicate a weaker covalent bonding interaction between C2 and C3 upon elongation of the interatomic distance. We also investigated the theoretical electron density distribution (EDD) in the space between C2 and C3. **Figure S12** shows the static model deformation density maps, which were obtained by a B3LYP-D3/6-311+G** calculation, based on the X-ray structures determined at 90, 100, 200, 300, and 400 K. As indicated, the deformation electron density between C2 and C3 decreased with increasing interatomic distance, and almost disappeared at a distance of 2.04 Å (at 90 K). Furthermore, as shown in **Fig. S13A**, the pyramidalisation angles (θ_p) of C2 and C3, which were determined by POAV analysis, gradually reduced from ~2° upon cooling, and the planarity of C2 and C3 became more pronounced below 200 K. This behaviour is in line with

the temperature dependence of the bond distance ($d_{C2\text{-}C3}$) between C2 and C3 (**Fig. S13B**), and it was found that C2 and C3 adopt a purer sp^2 hybridisation upon elongating $d_{C2\text{-}C3}$. Thus, the elongation of the C2–C3 bond to 2.04 Å can be regarded as coming close to the critical point of bond cleavage in terms of the electron density and molecular structure. However, considering that none of the properties shown in **Fig. 4** undergo an appreciable jump to indicate drastic changes in the bonding situation, a covalent bonding interaction still remains between C2 and C3, even with an interatomic distance of 2.04 Å.

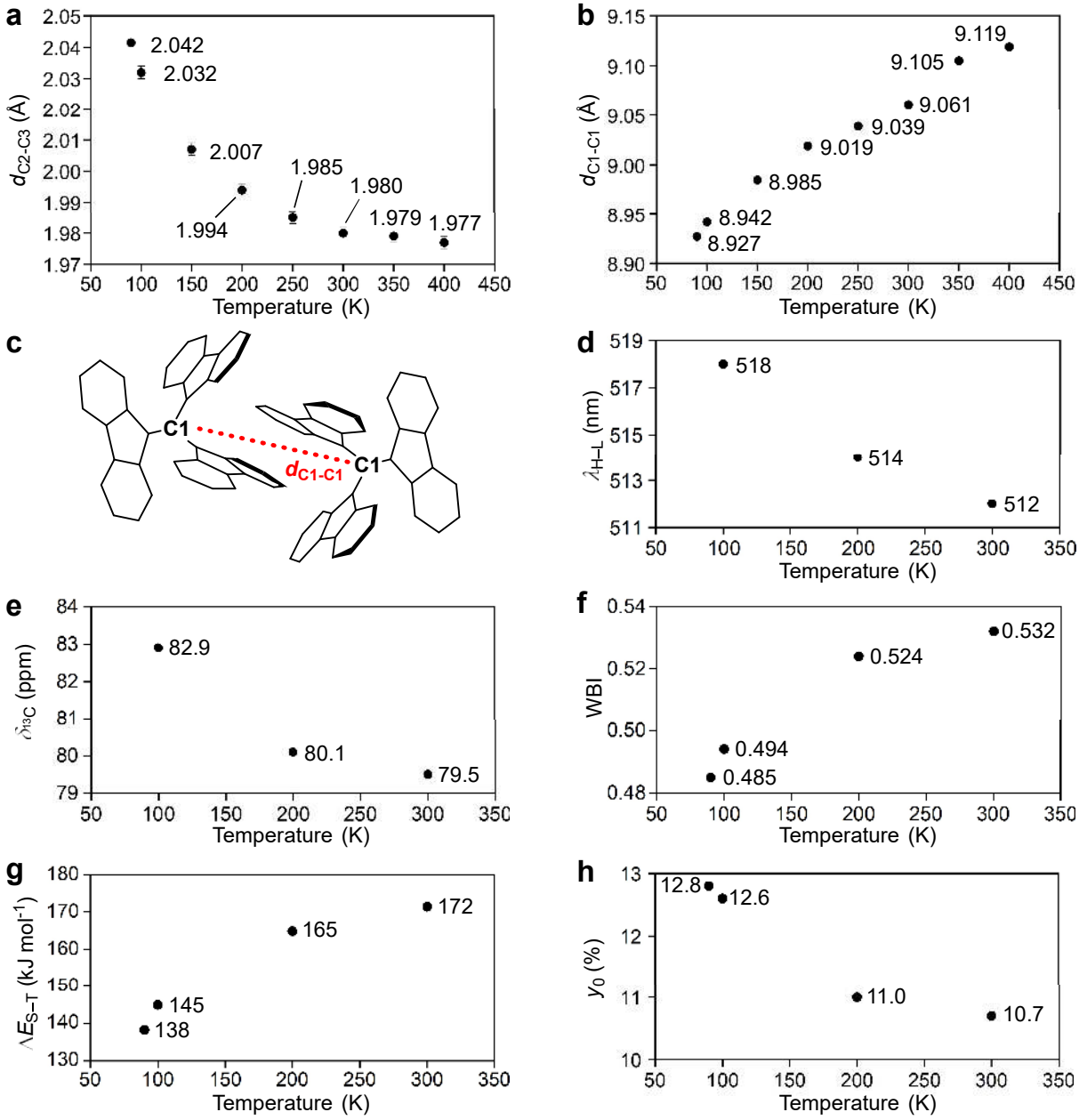

Fig. 4. Temperature dependence of the experimental and theoretical data of 1. a, Interatomic distance ($d_{C2–C3}$, Å) between C2 and C3. **b**, Interatomic distance ($d_{C1–C1}$, Å) between C1 and C1 in the dimeric pair. **c**, Definition of $d_{C1–C1}$ in the dimeric pair. **d**, Wavelength ($\lambda_{H–L}$, nm) of the HOMO→LUMO transition determined by polarised reflection measurements. **e**, ^{13}C NMR chemical shifts (δ_{13C}, ppm) of C2 and C3 determined by solid-state CP/MAS ^{13}C NMR measurements. **f**, Wiberg bond index (WBI) of C2–C3 estimated by a B3LYP-D3/6-311+G** calculation. **g**, Singlet–triplet energy gap ($\Delta E_{S–T}$, kJ mol^{-1}) determined by a B3LYP-D3/6-311+G** calculation. **h**, Diradical character (y_0, %) determined by a CASSCF(6,6)/6-311G* calculation.

In conclusion, to investigate the electronic structure between two distantly positioned carbon atoms in terms of a covalent bonding interaction, various experimental and theoretical analyses were employed since the existence (or not) of covalent bonding can depend on what is measured, and also on the criteria employed to identify a bond[35]. With the exception of the AIM model, all measurements and analyses carried out supported the presence of a sufficient covalent bonding interaction between C2 and C3, even with an interatomic distance beyond 2.0 Å. Importantly, in compound **1**, no diradical behaviour was detected for a long bond of 2.04 Å, but the structure and electron density of the molecule indicated possible bond cleavage. Exploring novel chemical behaviours associated with bond cleavage by investigating molecules with longer bonds will be of great significance in discovering new functionality and reactions of compounds.

References

1. Oliva, J. M., Allan, N. L., Schleyer, P. V. R., Viñas, C. & Teixidor, F. Strikingly long C···C distances in 1,2-disubstituted *ortho*-carboranes and their dianions. *J. Am. Chem. Soc.* **127**, 13538–13547 (2005).

2. Tanaka, K., Takamoto, N., Tezuka, Y., Kato, M. & Toda, F. Preparation and structural study of naphtho- and anthrocyclobutene derivatives which have extremely long C–C bonds. *Tetrahedron* **57**, 3761–3767 (2001).

3. Baldridge, K. K. *et al.* The Nature of the long bond in 3,8-dichloro-1,1,2,2-tetraphenylcyclobuta[*b*]naphthene. *J. Am. Chem. Soc.* **120**, 6167–6168 (1998).

4. Kammermeier, S., Herges, R. & Jones, P. G. [2+2] Cycloaddition products of tetradehydrodianthracene: Experimental and theoretical proof of extraordinary long C–C single bonds. *Angew. Chem. Int. Ed. Engl.* **36**, 1757–1760 (1997).

5. Yannoni, N., Kahr, B. & Mislow, K. Determination of the central bond length in hexaarylethanes by nutation NMR spectroscopy. *J. Am. Chem. Soc.* **110**, 6670–6672 (1988).

6. Kahr, B., Van Engen, D. & Mislow, K. Length of the ethane bond in hexaphenylethane and its derivatives. *J. Am. Chem. Soc.* **108**, 8305–8307 (1986).

7. Stein, M., Winter, W. & Rieker, A. Hexakis(2,6-di-*tert*-butyl-4-biphenylyl)ethane? The first unbridged hexaarylethane. *Angew. Chem. Int. Ed. Engl.* **17**, 692–694 (1978).

8. Schreiner, P. R. *et al.* Overcoming lability of extremely long alkane carbon–carbon bonds through dispersion forces. *Nature* **477**, 308–311 (2011).

9. Grimme, S. & Schreiner, P. R. Steric crowding can stabilize a labile molecule: Solving the hexaphenylethane riddle. *Angew. Chem. Int. Ed.* **50**, 12639–12642 (2011).

10. Fokin, A. A. *et al.* Stable alkanes containing very long carbon–carbon bonds. *J. Am. Chem. Soc.* **134**, 13641–13650 (2012).

11. Rösel, S., Balestrieri, C. & Schreiner, P. R. Sizing the role of London dispersion in the dissociation of all-*meta tert*-butyl hexaphenylethane. *Chem. Sci.* **8**, 405–410 (2017).

12. Rösel, S., Becker, J., Allen, W. D. & Schreiner, P. R. Probing the delicate balance between Pauli repulsion and London dispersion with triphenylmethyl derivatives. *J. Am. Chem. Soc.* **140**, 14421–14432 (2018).

13. Ishigaki, Y., Shimajiri, T., Takeda, T., Katoono, R. & Suzuki, T. Longest C–C single bond among neutral hydrocarbons with a bond length beyond 1.8 Å. *Chem* **4**, 795–806 (2018).

14. Li, J. *et al.* Exceptionally long C−C single bonds in diamino-*o*-carborane as induced by negative hyperconjugation. *Angew. Chem. Int. Ed.* **58**, 1397–1401 (2019).

15. Mandal, N., Pal, A. K., Gain, P., Zohaib, A. & Datta, A. Transition-state-like planar structures for amine inversion with ultralong C–C bonds in diamino-*o*-carborane and diamino-*o*-dodecahedron. *J. Am. Chem. Soc.* **142**, 5331–5337 (2020).

16. Hirshfeld, F. L. Can X-ray data distinguish bonding effects from vibrational smearing? *Acta Crystallogr. Sect. A* **32**, 239–244 (1976).

17. Barigelletti, F., Orlandi, G., Giro, G. & Poggi, G. Electron spin resonance study of γ-irradiated single crystals of fluorene. *J. Chem. Soc., Faraday Trans. 2* **71**, 1436–1439 (1975).

18. Hashizume, D. Experimental observation of the nature of weak chemical bonds in labile compounds. *Adv. Mater.* **29**, 1605175 (2017).

19. Schwarz, W. H. E., Ruedenberg, K. & Mensching, L. Chemical deformation densities. 1. Principles and formulation of quantitative determination. *J. Am. Chem. Soc.* **111**, 6926–6933 (1989).

20. Mensching, L., Von Niessen, W., Valtazanos, P., Ruedenberg, K. & Schwarz, W. H. E. Chemical deformation densities. 2. Small molecules. *J. Am. Chem. Soc.* **111**, 6933–6941 (1989).

21. Bader, R. F. W., Slee, T. S., Cremer, D. & Kraka, E. Description of conjugation and hyperconjugation in terms of electron distributions. *J. Am. Chem. Soc.* **105**, 5061–5068 (1983).

22. Mota, F., Miller, J. S. & Novoa, J. J. Comparative analysis of the multicenter, long bond in $[TCNE]^{\bullet-}$ and phenalenyl radical dimers: A unified description of multicenter, long bonds. *J. Am. Chem. Soc.* **131**, 7699–7707 (2009).

23. Kertesz, M. Pancake bonding: An unusual pi-stacking interaction. *Chem. Eur. J.* **25**, 400–416 (2019).

24. Bader, R. F. W. Atoms in molecules. *Acc. Chem. Res.* **18**, 9–15 (1985).

25. Lu, T. & Chen, F. Multiwfn: A multifunctional wavefunction analyzer. *J. Comput. Chem.* **33**, 580–592 (2012).

26. Haddon, R. C. Comment on the relationship of the pyramidalization angle at a conjugated carbon atom to the σ bond angles. *J. Phys. Chem. A* **105**, 4164–4165 (2001).

27. Lodewyk, M. W., Siebert, M. R. & Tantillo, D. J. Computational prediction of ^{1}H and ^{13}C chemical shifts: A useful tool for natural product, mechanistic, and synthetic organic chemistry. *Chem. Rev.* **112**, 1839–1862 (2012).

28. Ditchfield, R. Self-consistent perturbation theory of diamagnetism. *Mol. Phys.* **27**, 789–807 (1974).

29. Wolinski, K., Hinton, J. F. & Pulay, P. Efficient implementation of the gauge-independent atomic orbital method for NMR chemical shift calculations. *J. Am. Chem. Soc.* **112**, 8251–8260 (1990).

30. Debroy, P., Lindeman, S. V. & Rathore, R. Hexabenzo[4.4.4]propellane: A helical molecular platform for the construction of electroactive materials. *Org. Lett.* **9**, 4091–4094 (2007).

31. Palomas, D. *et al.* Synthesis and reactivity of electron poor allenes: Formation of completely organic frustrated Lewis pairs. *Dalton Trans.* **41**, 9073–9082 (2012).

32. Doehnert, D. & Koutecky, J. Occupation numbers of natural orbitals as a criterion for biradical character. Different kinds of biradicals. *J. Am. Chem. Soc.* **102**, 1789–1796 (1980).

33. Winkler, M. & Sander, W. The Structure of *meta*-benzyne revisited – A close look into σ-bond formation. *J. Phys. Chem. A* **105**, 10422–10432 (2001).

34. Wei, H., Hrovat, D. A., Mo, Y., Hoffmann, R. & Borden, W. T. The contributions of through-bond interactions to the singlet−triplet energy difference in 1,3-dehydrobenzene. *J. Phys. Chem. A* **113**, 10351–10358 (2009).

35. Ball, P. Beyond the bond. *Nature* **469**, 26–28 (2011).

Data availability

The authors declare that the data supporting the findings of this study are available within the paper and its Supplementary Information. X-ray data are available free of charge from the Cambridge Crystallographic Data Centre under reference CCDC-1995679 (**1** at 90 K), 2062007 (**1** at 100 K), 2062017 (**1** at 150 K), 1995680 (**1** at 200 K), 2062018 (**1** at 250 K), 2062019 (**1** at 300 K), 2062024 (**1** at 350 K), 2062025 (**1** at 400 K), 1995682 (**3**), and 1995683 (**2a**). Further spectroscopic, crystallographic, and computational data are included in the Supplementary Information.

Acknowledgments

T.K. thanks the JSPS for KAKENHI funding (Grant No. JP18H01965) and a Grant-in-Aid for Transformative Research Areas (A) “Condensed Conjugation” (JSPS for KAKENHI funding Grant No. JP20H05865) from MEXT, Japan. H.O. thanks the JSPS for KAKENHI funding (Grand No. JP18H01166) and the Japan Science and Technology Agency (JST) for CREST funding (Grant No. JPMJCR1661).

Author contributions

T.K. conceptualised and supervised the research; Y.S. conducted the preparation and formal analysis of compounds; D.H. conducted the X-ray investigation; H.S., T.M., and H.O. conducted the polarised reflection measurements; K.R. and N.M. conducted theoretical calculations; T.K. wrote the original draft; T.K. D.H. H.O., and N.M. reviewed and edited the subsequent drafts.

Competing interests

The authors declare no conflicts of interest.

Additional information

Supplementary Information is available for this paper at xxx.

Correspondence and requests for materials should be addressed to T.K.

Reprints and permissions information is available at www.nature.com/reprints.

Figures

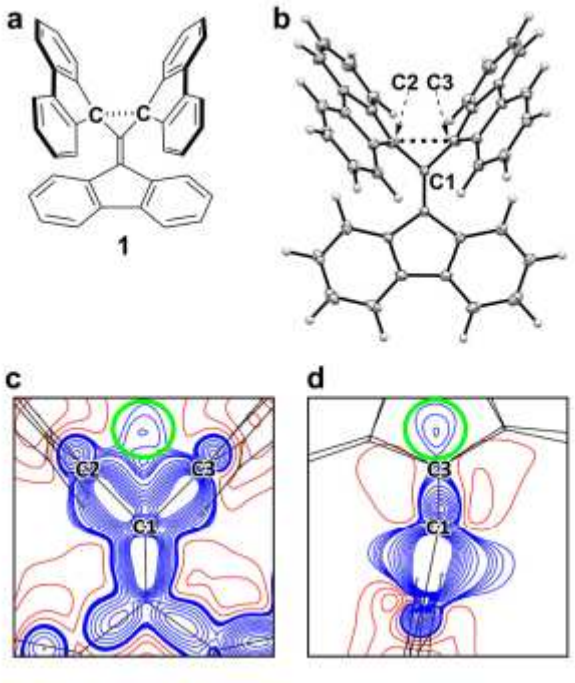

Figure 1

Structure of 1. a, Chemical structure of 1. b, An ORTEP drawing of 1 at 90 K. Thermal ellipsoids are drawn at the 50% probability level. c, Static model deformation density maps on the C1-C2-C3 plane, and d, cross-sectional view of the C1-C2-C3 plane along the line connecting C1 and the midpoint between the C2 and C3 atoms. The concentration of electron density between C2 and C3 is marked by a green circle. The blue lines represent positive contours from 0.01 to 0.05 e Å−3 in steps of 0.01 e Å−3 and from 0.10 to 0.50 e Å−3 in steps of 0.05 e Å−3 . The red lines represent negative contours from −0.05 to −0.50 in steps of −0.05 e Å−3.

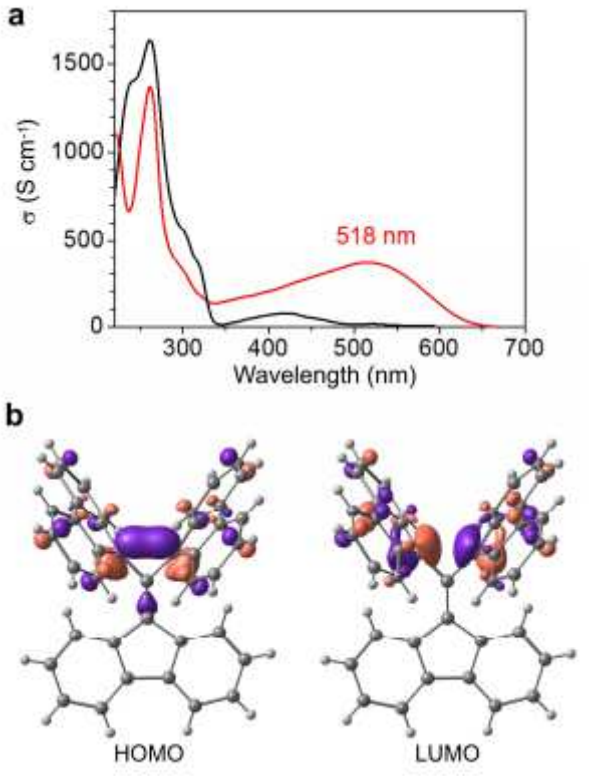

Figure 2

Evaluation of the electron–electron interaction between C2 and C3. a, Optical conductivity (σ) spectra of 1 at 100 K obtained with light polarised along (red solid line) and perpendicular to (black solid line) the a-axis on the single crystal (001) face. b, HOMO and LUMO of 1 (90 K) calculated using the B3LYP-D3/6-311+G** method. Purple and light red surfaces represent the relative signs of the orbital coefficients drawn at the 0.4 e Å−3 (= 0.06 e au−3) level.

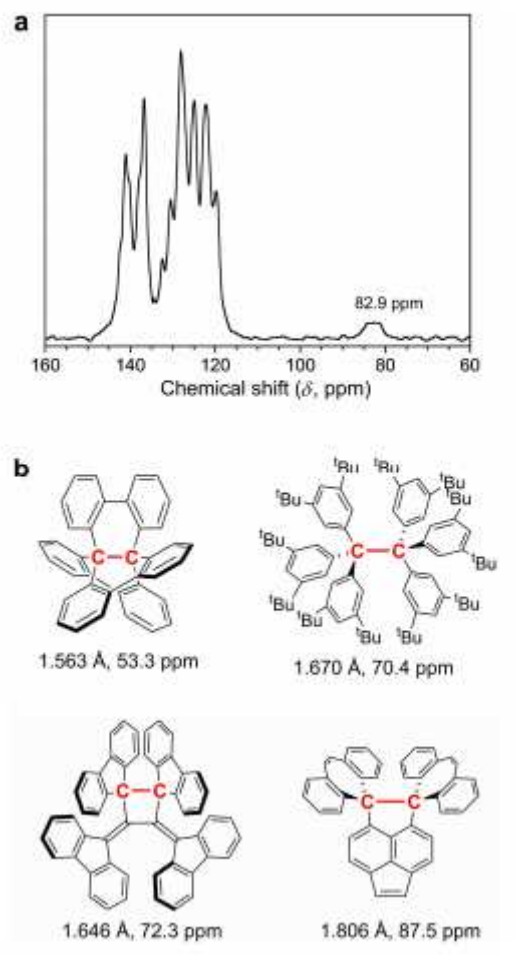

Figure 3

13C NMR chemical shifts. a, Solid-state CP/MAS 13C NMR spectrum of powdered 1 measured at 100 K. b, Bond distances and 13C chemical shifts at the sp3 benzylic carbons (shown in red) of selected aromatic hydrocarbon compounds.

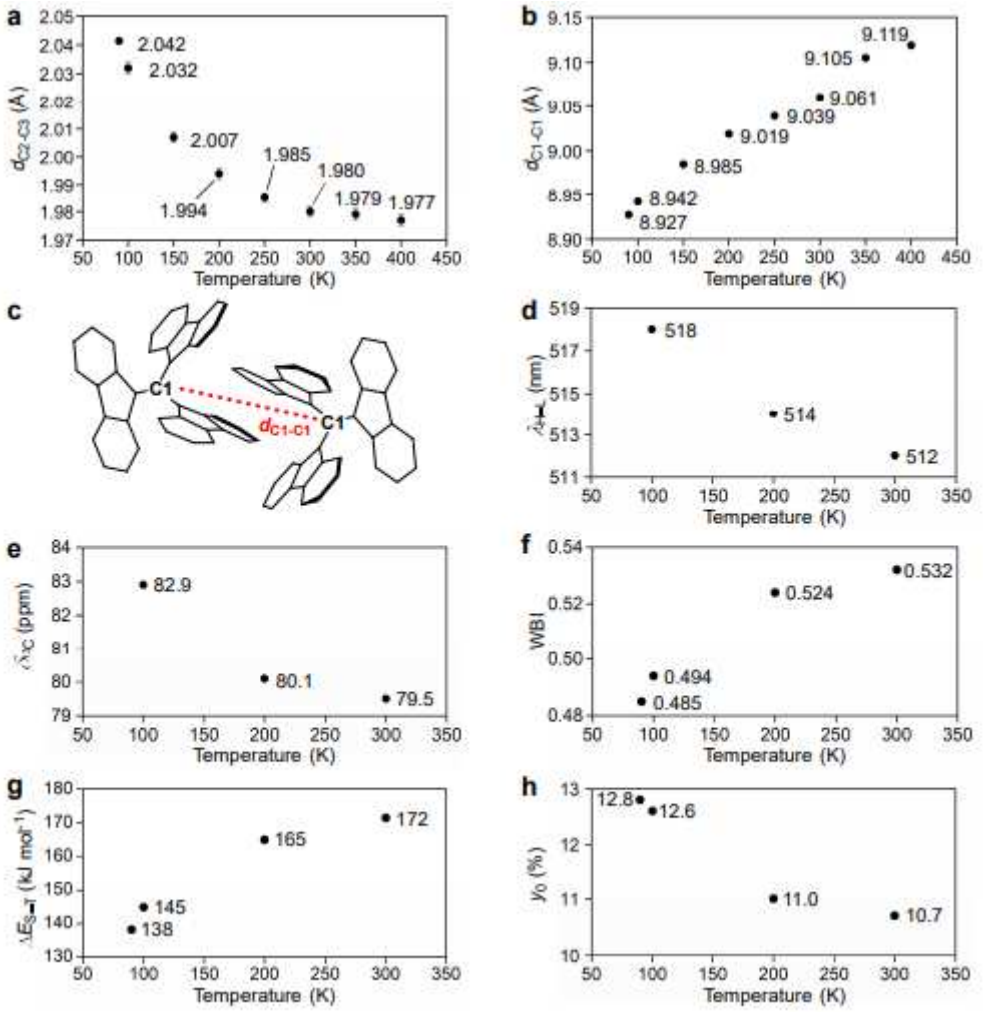

Figure 4

Temperature dependence of the experimental and theoretical data of 1. a, Interatomic distance (dC2–C3, Å) between C2 and C3. b, Interatomic distance (dC1–C1, Å) between C1 and C1 in the dimeric pair. c, Definition of dC1–C1 in the dimeric pair. d, Wavelength (λH–L, nm) of the HOMO□LUMO transition determined by polarised reflection measurements. e, 13C NMR chemical shifts (δ13C, ppm) of C2 and C3 determined by solidstate CP/MAS 13C NMR measurements. f, Wiberg bond index (WBI) of C2–C3 estimated by a B3LYP-D3/6-311+G** calculation. g, Singlet–triplet energy gap (ΔES–T, kJ mol–1) determined by a B3LYP-D3/6-311+G** calculation. h, Diradical character (y0, %) determined by a CASSCF(6,6)/6-311G* calculation.

Supplementary Files

This is a list of supplementary files associated with this preprint. Click to download.

- SupplementaryInformation.pdf
- checkCIFs.zip

- CIFs.zip